Journal of Instrumentation

OPEN ACCESS

Rigorous mathematical modelling for a Fast Corrector Power Supply in TPS

Published by IOP Publishing for Sissa Medialab

Received: *February 21, 2017*
Accepted: *March 17, 2017*
Published: *April 13, 2017*

TECHNICAL REPORT

Rigorous mathematical modelling for a Fast Corrector Power Supply in TPS

K.-B. Liu, C.-Y. Liu,[1] Y.-C. Chien, B.-S. Wang and Y.S. Wong

National Synchrotron Radiation Research Center,
Hsinchu 30076, Taiwan

E-mail: cyl@nsrrc.org.tw

Abstract: To enhance the stability of beam orbit, a Fast Orbit Feedback System (FOFB) eliminating undesired disturbances was installed and tested in the 3rd generation synchrotron light source of Taiwan Photon Source (TPS) of National Synchrotron Radiation Research Center (NSRRC). The effectiveness of the FOFB greatly depends on the output performance of Fast Corrector Power Supply (FCPS); therefore, the design and implementation of an accurate FCPS is essential. A rigorous mathematical modelling is very useful to shorten design time and improve design performance of a FCPS. A rigorous mathematical modelling derived by the state-space averaging method for a FCPS in the FOFB of TPS composed of a full-bridge topology is therefore proposed in this paper. The MATLAB/SIMULINK software is used to construct the proposed mathematical modelling and to conduct the simulations of the FCPS. Simulations for the effects of the different resolutions of ADC on the output accuracy of the FCPS are investigated. A FCPS prototype is realized to demonstrate the effectiveness of the proposed rigorous mathematical modelling for the FCPS. Simulation and experimental results show that the proposed mathematical modelling is helpful for selecting the appropriate components to meet the accuracy requirements of a FCPS.

Keywords: Simulation methods and programs; Analogue electronic circuits; Modular electronics

[1]Corresponding author.

doi:10.1088/1748-0221/12/04/T04004

Contents

1 Introduction

For advanced scientific investigations in the related fields of molecular, material and medicine etc., the 3$^{\text{rd}}$ generation synchrotron light source of Taiwan Photon Source (TPS) in National Synchrotron Radiation Research Center (NSRRC), a 3 GeV synchrotron facility with very low emittance and ultra-brightness beam source, was constructed and operated since 2014. TPS is a concentric ring where booster and storage rings are built in the same tunnel. The booster ring is used to ramp the electron beam with 150 MeV from a linear accelerator up to 3 GeV at a 3 Hz repetition rate. The storage ring composed of 24 double-bend cells with 6-fold symmetry in a circumference of 518.4 m is then used to extract the electron beam. Due to the small beam sizes both in vertical and horizontal planes, the beam position control has to be in the order of tens of μm and therefore the requirement for the accuracy and stability of beam orbit is high. In order to enhance the accuracy and stability of beam orbit, a Fast Orbit Feedback System (FOFB) composed of corrector magnets, power supplies, beam position data and orbit compensation algorithm was installed and tested in TPS since 2015. The FOFB system can be used to eliminate undesired disturbances coming from magnetic strength errors, alignment errors and water pipe vibrations close to magnets etc. and to suppress the beam orbit instability [1, 2].

The effectiveness of the FOFB greatly depends on the output performance of Fast Corrector Power Supply (FCPS) for corrector magnet; therefore, the design and implementation of a high accurate FCPS is essential. To achieve high accuracy and stability for a FCPS, some optimal design issues such as the selection of circuit components, the adjustment of controller parameters, the influences of uncertainties in the current sensor and circuit components on output stability and so on should be considered and integrated into a FCPS design. In general, the commonly-used circuit simulation software including PSCAD, Spice, and PSIM etc. can be used for transient-behavior simulation of a FCPS; however, the software cannot be straightforwardly used to select the circuit components, adjust the parameters of controller and especially revolve the effects of uncertainties in the current sensor and circuit components on output stability. The design of a high accurate FCPS is therefore very time-consuming since many factors need to be premeditated and investigated. A rigorous mathematical modelling is indispensable for shortening design time and improving design performance of a FCPS [3, 4].

A rigorous mathematical modelling derived by the state-space averaging method for a FCPS in the FOFB of TPS composed by a full-bridge topology is proposed in this paper. The MATLAB/SIMULINK software is used to construct the proposed mathematical modelling and to conduct the simulations of the proposed FCPS. The proposed mathematical modelling for the FCPS can be used to select the appropriate components to meet the accuracy requirements of the FCPS. As a case study, the simulations for the effects of different resolutions (bits) of ADC on the output accuracy of the FCPS in the FOFB of TPS are investigated. Simulation results demonstrate the effectiveness and efficiency of using the proposed mathematical modelling for the optimal design of the FCPS.

2 Basic circuit and operations of a FCPS

Figure 1 shows the basic circuit configuration of the FCPS in the FOFB of TPS designed and developed by the power supply group of NSRRC. The ±10 A/±50 V FCPS employs the full-bridge topology where V_{DC} is the input DC voltage; S_1 to S_4 are the MOSFETs; L_{f1}, L_{f2} and C_f constitute a low-pass filter; L_M and R_M are the equivalent load of a corrector magnet; and *Shunt* is a high precision shunt resistor used as current sensor. A Hybrid Pulse Width Modulation (HPWM) as proposed in [5] requiring two of the four MOSFETs in the full-bridge circuit to be operated at high frequency and the other two be switched at the output frequency is adopted in this paper. Since only two of the four MOSFETs are switched at high frequency, the switching loss can be reduced effectively. The HPWM was designed based on the conventional unipolar PWM which compares a sinusoidal reference signal with a triangular carrier signal to generate the PWMs for MOSFETs. Figure 2 illustrates the theoretical PWM control signals for the MOSFETs S_1 to S_4 and the bridge output voltage assuming that S_1 and S_2 are operated at output frequency and S_3 and S_4 are switched at high frequency. In figure 2, V_{sin} and $V_{\mathrm{sin\_inv}}$ are the sinusoidal reference signals for the positive and negative bridge output voltages, respectively; V_{tri} is the triangular carrier signal; PWM_{S1} to PWM_{S4} are the corresponding PWM control signals for MOSFETs S_1 to S_4; and V_{ab} is the bridge output voltage.

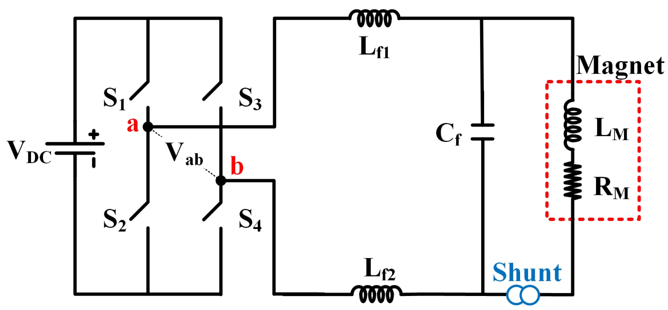

Figure 1. Basic circuit configuration of a full-bridge FCPS.

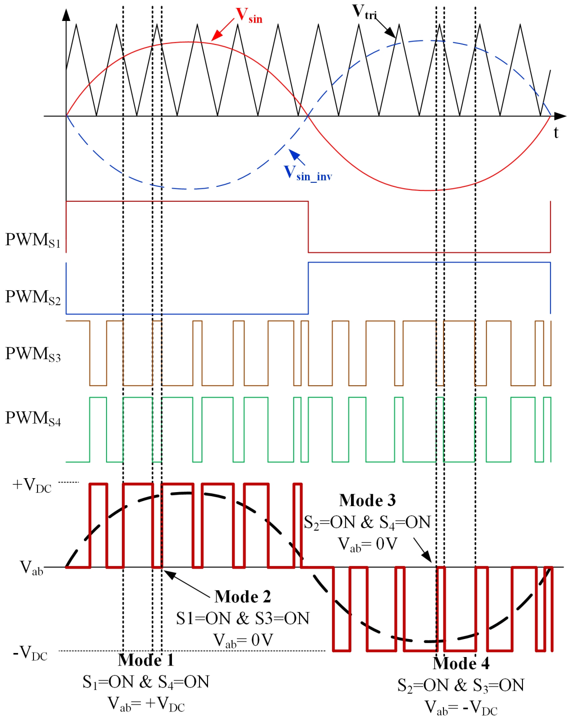

Figure 2. Key waveforms of the full-bridge FCPS.

It can be observed from figure 2 that PWM_{S2} and PWM_{S4} are complementary to PWM_{S1} and PWM_{S3}. There are four operational modes in the FCPS. Figure 3 shows the equivalent circuits of modes 1 and 2 for the positive bridge output voltage. As shown in figures 2 and 3(a), mode 1 represents that V_{sin} is larger than 0 and V_{sin} is larger than V_{tri} with PWM_{S1}, PWM_{S2}, PWM_{S3} and PWM_{S3} being in the ON, OFF, OFF and ON states, respectively, and the bridge output voltage V_{ab} being $+V_{\mathrm{DC}}$. Similarly, mode 2 denotes that V_{sin} is smaller than 0 and V_{sin} is larger than V_{tri} demonstrated in figures 2 and 3(b), with PWM_{S1}, PWM_{S2}, PWM_{S3} and PWM_{S3} being in the ON, OFF, ON and OFF states, respectively, and the bridge output voltage V_{ab} being 0. Modes 3 and 4 which are similar to modes 2 and 1 belong to the negative bridge output and the details are abridged.

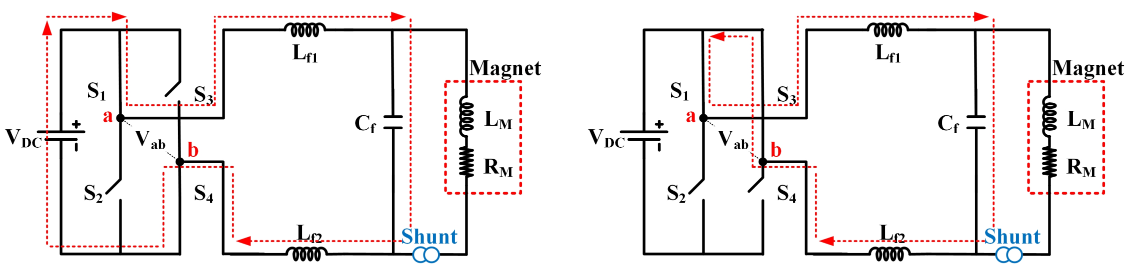

(a) Mode 1 **(b)** Mode 2

Figure 3. Operational modes of the proposed FCPS.

3 Rigorous mathematical modelling of a FCPS

To achieve high accuracy and stability in the FCPS, a rigorous mathematical modelling is derived in this paper to simulate some optimal design issues for the FCPS and therefore to shorten design time and improve design performance. The state-space averaging method that has been widely applied to model power electronic circuits is used in this paper. The state-space averaging method uses the state variables to derive the state equation for the equivalent circuit of each switching mode and then average the state equations using duty cycle to obtain the state-space averaging equation. The transfer function aiming for the stability analysis and optimal parameters design of controller can be solved by the derived state-space averaging equation.

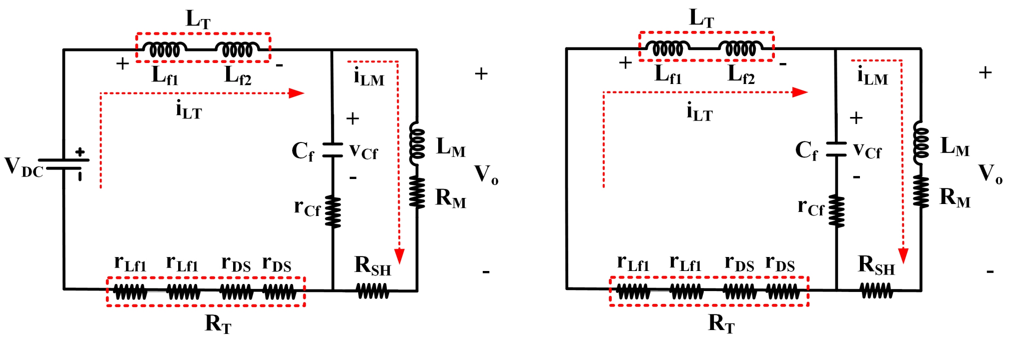

(a) Mode 1 **(b)** Mode 2

Figure 4. Equivalent circuits of operational modes.

Figure 4 shows the equivalent circuits of modes 1 and 2 where r_{fL1} and r_{fL2} are the DC impedances for L_{f1} and L_{f2}; r_{Cf} is the equivalent series resistance of C_f; r_{DS} is the drain-source resistance of a MOSFET; and R_{SH} is the shunt resistor of the current sensor. For simplicity, the summations of L_{f1} and L_{f2} and of r_{fL1}, r_{fL2}, r_{DS} and r_{DS} are denoted as L_T and R_T, respectively. From figure 4, it can be observed that the state variables for the FCPS are i_{LT}, i_{LM}, and v_{Cf}. Using Kirchhoff circuit laws, eq. (3.1) can be derived.

$$V_{\mathrm{DC}} = L_T \frac{di_{LT}}{dt} + i_{LT} R_T + v_{Cf} + (i_{LT} - i_{LM}) r_{Cf} \tag{3.1a}$$

$$L_M \frac{di_{LM}}{dt} + (R_{\mathrm{SH}} + R_M) i_{LM} = r_{Cf} (i_{LT} - i_{LM}) + v_{Cf} \tag{3.1b}$$

$$i_{LT} = C_f \frac{dv_{Cf}}{dt} + i_{LM} \tag{3.1c}$$

The output voltage can be expressed as

$$V_o = (i_{LT} - i_{LM}) r_{Cf} + v_{Cf} + R_{\mathrm{SH}} i_{LM} \tag{3.2}$$

The state equation for mode 1 can be rearranged from (3.1) and (3.2) and expressed as

$$\begin{bmatrix} \frac{di_{LT}}{dt} \\ \frac{di_{LM}}{dt} \\ \frac{dv_{Cf}}{dt} \end{bmatrix} = \begin{bmatrix} -\frac{(R_T + r_{Cf})}{L_T} & \frac{r_{Cf}}{L_T} & -\frac{1}{L_T} \\ \frac{r_{Cf}}{L_M} & -\frac{(R_{\mathrm{SH}} + R_M + r_{Cf})}{L_M} & \frac{1}{L_M} \\ \frac{1}{C_f} & -\frac{1}{C_f} & 0 \end{bmatrix} \begin{bmatrix} i_{LT} \\ i_{LM} \\ v_{Cf} \end{bmatrix} + \begin{bmatrix} \frac{1}{L_T} & 0 & 0 \end{bmatrix}^T [V_{\mathrm{DC}}] \tag{3.3a}$$

$$[V_o] = \begin{bmatrix} r_{Cf} & (R_{\mathrm{SH}} - r_{Cf}) & 1 \end{bmatrix} \begin{bmatrix} i_{LT} \\ i_{LM} \\ v_{Cf} \end{bmatrix} \tag{3.3b}$$

2017 JINST 12 T04004

Eq. (3.3) can be rewritten as

$$\begin{aligned}\mathbf{x}(\mathbf{t}) &= \mathbf{A_1 x}(\mathbf{t}) + \mathbf{B_1 u}(\mathbf{t}) \\ \mathbf{y}(\mathbf{t}) &= \mathbf{C_1 x}(\mathbf{t}) + \mathbf{D_1 u}(\mathbf{t})\end{aligned} \tag{3.4a}$$

$$\mathbf{x} = \begin{bmatrix} i_{LT} & i_{LM} & v_{Cf} \end{bmatrix}^T \tag{3.4b}$$

$$\mathbf{y} = [V_o] \tag{3.4c}$$

$$\mathbf{u} = [V_{\mathrm{DC}}] \tag{3.4d}$$

$$\mathbf{A_1} = \begin{bmatrix} -\frac{(R_T + r_{Cf})}{L_T} & \frac{r_{Cf}}{L_T} & -\frac{1}{L_T} \\ \frac{r_{Cf}}{L_M} & -\frac{(R_{\mathrm{SH}} + R_M + r_{Cf})}{L_M} & \frac{1}{L_M} \\ \frac{1}{C_f} & -\frac{1}{C_f} & 0 \end{bmatrix} \tag{3.4e}$$

$$\mathbf{B_1} = \begin{bmatrix} \frac{1}{L_T} & 0 & 0 \end{bmatrix}^T \tag{3.4f}$$

$$\mathbf{C_1} = \begin{bmatrix} r_{Cf} & (R_{\mathrm{SH}} - r_{Cf}) & 1 \end{bmatrix} \tag{3.4g}$$

$$\mathbf{D_1} = [0] \tag{3.4h}$$

Using the similar procedures as derived in (3.1) to (3.3), the state equation for mode 2 as shown in figure 4(b) can be expressed as

$$\begin{aligned}\mathbf{x}(\mathbf{t}) &= \mathbf{A_2 x}(\mathbf{t}) + \mathbf{B_2 u}(\mathbf{t}) \\ \mathbf{y}(\mathbf{t}) &= \mathbf{C_2 x}(\mathbf{t}) + \mathbf{D_2 u}(\mathbf{t})\end{aligned} \tag{3.5a}$$

$$\mathbf{A_2} = \mathbf{A_1} \tag{3.5b}$$

$$\mathbf{B_2} = \begin{bmatrix} 0 & 0 & 0 \end{bmatrix}^T \tag{3.5c}$$

$$\mathbf{C_2} = \mathbf{C_1} \tag{3.5d}$$

$$\mathbf{D_2} = \mathbf{D_1} \tag{3.5e}$$

Let T_S be one switching period and dT_S and $d'T_S$ be the turn-on time and turn-off time for modes 1 and 2 in the switching period as illustrated figure 4, respectively, the state equations for mode 1 and mode 2 as expressed in (3.4a) and (3.5a) can then be rewritten approximately as (3.6) and (3.7), respectively.

$$\frac{\mathbf{x}(dT_S) - \mathbf{x}(0)}{dT_S} = \mathbf{A_1 x} + \mathbf{B_1 u} \tag{3.6a}$$

$$dT_S \mathbf{y} = dT_S \mathbf{C_1 x} + dT_S \mathbf{D_1 u} \tag{3.6b}$$

$$\frac{\mathbf{x}(T_S) - \mathbf{x}(dT_S)}{d'T_S} = \mathbf{A_2 x} + \mathbf{B_2 u} \tag{3.7a}$$

$$d'T_S \mathbf{y} = d'T_S \mathbf{C_2 x} + d'T_S \mathbf{D_2 u} \tag{3.7b}$$

The state equation for one switching period can be obtained approximately by averaging the state equations for modes 1 and 2 expressed in (3.6) and (3.7), they are

$$\frac{\mathbf{x}(T_S) - \mathbf{x}(\mathbf{0})}{T_S} = d(\mathbf{A_1 x} + \mathbf{B_1 u}) + d'(\mathbf{A_2 x} + \mathbf{B_2 u}) \tag{3.8a}$$

$$\frac{dT_S \mathbf{y_1} + d'T_S \mathbf{y_2}}{T_S} = d\mathbf{C_1 x} + d\mathbf{D_1 u} + d'\mathbf{C_2 x} + d'\mathbf{D_2 u} \tag{3.8b}$$

Therefore, the state-space averaging equation can be written as

$$\begin{aligned} \mathbf{x}(\mathbf{t}) &= \mathbf{Ax}(\mathbf{t}) + \mathbf{Bu}(\mathbf{t}) \\ \mathbf{y}(\mathbf{t}) &= \mathbf{Cx}(\mathbf{t}) + \mathbf{Du}(\mathbf{t}) \end{aligned} \tag{3.9a}$$

$$\mathbf{A} = d\,(\mathbf{A_1}) + d'\,(\mathbf{A_2}) \tag{3.9b}$$

$$\mathbf{B} = d\,(\mathbf{B_1}) + d'\,(\mathbf{B_2}) \tag{3.9c}$$

$$\mathbf{C} = d\,(\mathbf{C_1}) + d'\,(\mathbf{C_2}) \tag{3.9d}$$

$$\mathbf{D} = d\,(\mathbf{D_1}) + d'\,(\mathbf{D_2}) \tag{3.9e}$$

$$d = 1 - d' \tag{3.9f}$$

The stat-space averaging equations obtained by (3.9) can be integrated into optimal design of the FCPS. Figure 5 illustrates the simulation architecture for the FCPS using state-space averaging equation where i_{LM}^{MEA} is the current signal acquired from the shunt resistor and signal acquisition module; i_{LM}^{ADC} is the digital current signal obtained by the ADC module; and i_{LM}^{COM} is the current command used for Proportional-Integral (PI) controller. From figure 5, it can be observed that the effects of the DC impedances of L_{f1} and L_{f2}, the equivalent series resistance of C_f, the drain-source resistance of a MOSFET and the shunt resistor of the current sensor on the output performance of the FCPS can be effectively analyzed in the proposed simulation architecture. Besides, the uncertainties in the signal acquisition module and ADC module can also be investigated. Therefore, some optimal design issues such as the selection of circuit components, the adjustment of controller parameters, the effects of uncertainties in the current/voltage sensors and circuit components on the output stability and so on can be considered and integrated into the FCPS design using the derived state-space averaging equation and the proposed simulation architecture.

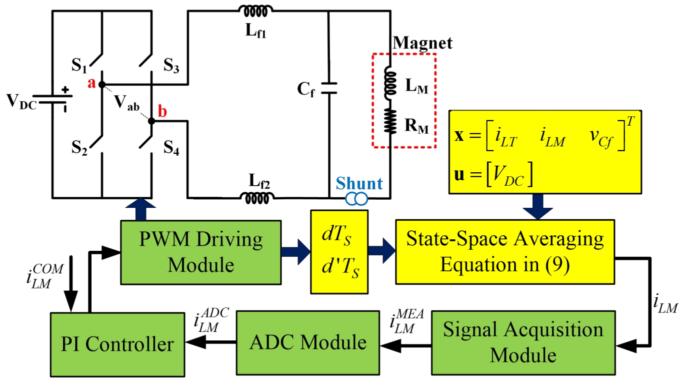

Figure 5. Simulation architecture for a FCPS.

4 Simulation and experimental results

The MATLAB/SIMULINK software is used to construct the proposed mathematical modelling and to conduct the simulations of the FCPS. Figure 6 shows the simulation block diagram constructed by MATLAB/SIMULINK software. Table 1 lists the circuit parameters used in the designed FCPS. The proposed simulation architecture can be used to design and select the components for the deigned FCPS. As a case, the simulations for the effects of the different resolutions of ADC on the output accuracy of the proposed FCPS are investigated. The rated output current i_{LM} is ± 10 A.

2017 JINST 12 T04004

The output current is transformed to an input voltage in ±0.1 V for the signal acquisition module by the shunt resistor. The output current signal i_{LM}^{MEA} is in ±10 V and the ADC module with the input range of ±12 V is used to convert the analog output current signal i_{LM}^{MEA} to the digital current signal i_{LM}^{ADC}. The accuracy requirement for the output current i_{LM} is that the mean error must be lower than 10 ppm (100 uA) at 10 A.

The maximum round-off error for an ADC module with the input range of ±12 V can be calculated by

$$\mathrm{ADC}_N^{\mathrm{error}} = \frac{24}{2^{N+1}} \tag{4.1}$$

where N is the number of bits for the ADC module.

The 12, 14, 16, 18 and 20-bit ADC modules are simulated by the proposed architecture. The maximum round-off errors for the different bits are listed in table 2. From (4.1) and table 2, the digital values in integer format, the floating values (V) and the round-off errors (V) for input value 10 V converted by the 12, 14, 16, 18 and 20-bit ADC modules are shown in table 3. Obviously, the larger number of bit for the ADC module has lower round-off error; however, it causes greater computational burden in the controller performance. Therefore, the appropriate number of bit for the ADC module needs to be designed thoughtfully. The proposed simulation architecture as shown in figure 6 can effectively take the influences of different bits of the ADC module on the output current accuracy into account. Besides, the components and parameters in the FCPS such as PI parameters in the controller also affect the output current accuracy and stability, thus needing to be considered together.

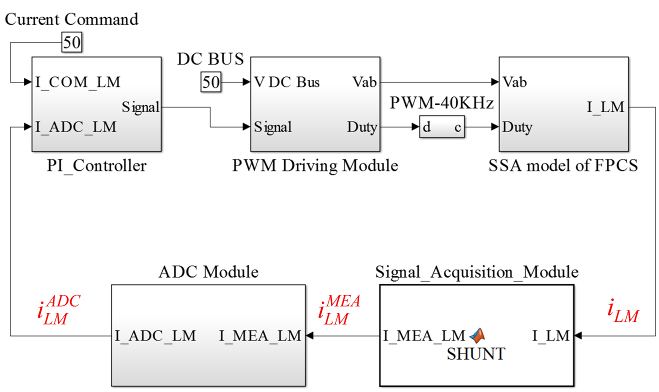

Figure 6. Simulation block diagram in MATLAB/SIMULINK.

Table 4 shows the performances of different bits of ADC module for the accuracy and stability of the designed FCPS at rated output current 10 A where mean, standard, min and max denote the mean, standard deviation, minimum and maximum values of the output current, respectively and the mean error indicates mean error value of output current. In table 4, it can be observed that the 16, 18 and 20-bit ADC modules can meet the accuracy requirement of the mean error of output current being lower than 10 ppm (100 uA) at 10 A. Comparing table 4 with tables 2 and 3, it can also be seen that the 16-bit ADC module has larger round-off error; however, the mean error obtained from the simulations is less than 10 ppm. Meanwhile, the 18-bit ADC module has about 4 times larger round-off error than that of the 20-bit ADC module; however, the simulated mean errors for

Table 1. Circuit parameters used in the designed FCPS.

L_{f1}/L_{f2}	200 μH
r_{Lf1}/r_{Lf2}	10 mΩ
C_f	1.23 uF
r_{Cf}	10 mΩ
r_{DS}	10.8 mΩ
R_M	0.395 mΩ
L_M	22.29 mH
R_{SH}	100 mΩ
f_s	40 kHz
V_{DC}	50 V

f_s is the switching frequency for MOSFETs operated at high frequency.

Table 2. Maximum round-off errors for different ADC modules.

Bits of ADC Module	Resolution (±12 V)
12	5859.375 uV
14	1464.843 uV
16	366.210 uV
18	91.552 uV
20	22.888 uV

Table 3. Digital values and error at the output current 10 A.

Bits of ADC Module	Input Value (V)	Digital Value (Int)	Floating Value (V)	Round-off Error (V)
12 Bits	10	3755	10.001953125	0.001953125
14 Bits	10	15019	10.000488281	0.000488281
16 Bits	10	60075	10.000122070	0.000122070
18 Bits	10	240299	10.000030517	0.000030517
20 Bits	10	961195	10.000007629	0.000007629

the 18 and 20-bit ADC modules are close. The computational performance of controller and PI parameters used in the controller may be the main reasons resulting in the differences. Figures 7–9 illustrate the simulated output current spectra for the 16, 18 and 20-bit ADC modules, respectively. From figures 7–9, it can be seen that the output current errors for the 16, 18 and 20-bit ADC module from 0 Hz to 1.6 kHz are lower than 10 ppm. Since the performance of the 18-bit ADC module is close to the 20-bit ADC module, the 18-bit ADC module is selected and used in the designed FCPS. Figure 10 shows the realized FCPS prototype using the 18-bit TI ADS8382. Figure 11 illustrates the measured output current spectrum from 0Hz to 1.6 kHz. From figure 11, it can be seen that the output current error of realized FCPS prototype is far less than 10 ppm; therefore, the effectiveness of the proposed rigorous mathematical modelling for the FCPS can be proved.

2017 JINST 12 T04004

Table 4. Performance of different bit numbers of ADC module for the accuracy and stability of the proposed FCPS.

	20 Bits	18 Bits	16 Bits	14 Bits	12 Bits
Mean	9.999976206	9.99996503	9.99992035	9.99974159	9.9990266
Standard Deviation	0.0000398	0.00004016	0.00004167	0.0000467	0.0000671
Min	9.999908232	9.99989651	9.999849247	9.99966178	9.99891212
Max	10.00004418	10.00003356	9.999991444	9.99982140	9.99914117
Mean Error	**23.79 uA (<10 ppm)**	**34.97 uA (<10 ppm)**	**79.65 uA (<10 ppm)**	**258 uA (>10 ppm)**	**973 uA (>10 ppm)**

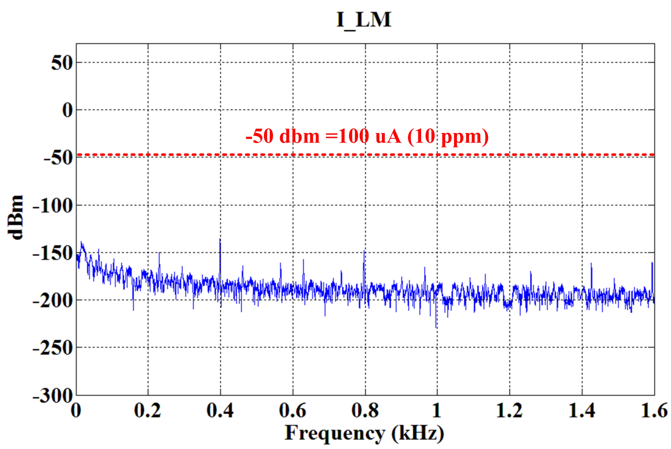

Figure 7. Output current spectrum for the 16-bit ADC.

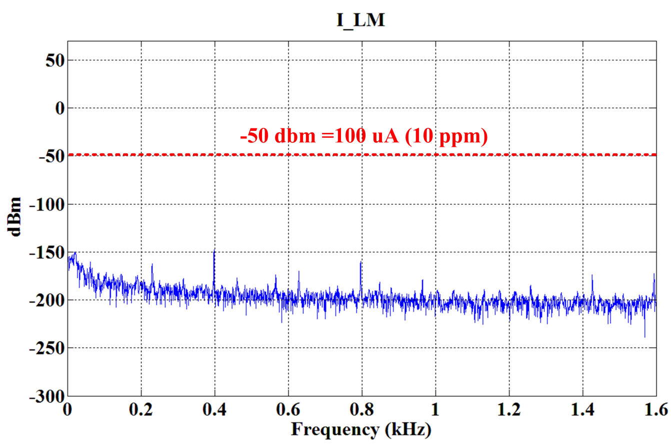

Figure 8. Output current spectrum for the 18-bit ADC.

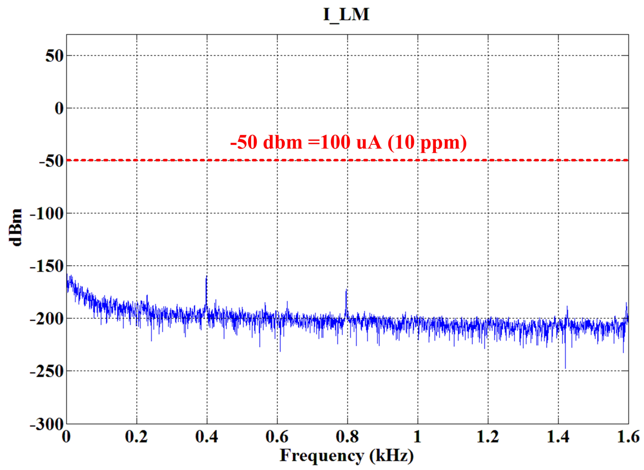

Figure 9. Output current spectrum for the 20-bit ADC.

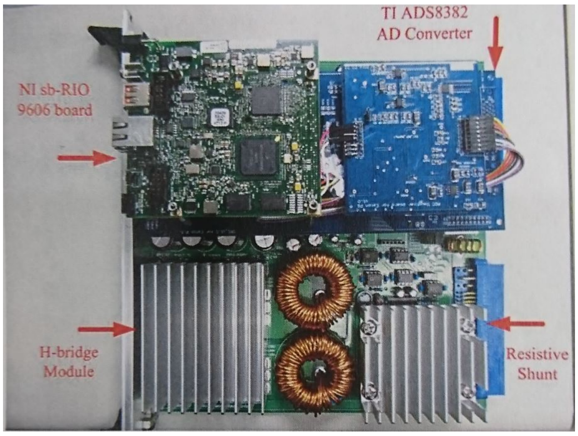

Figure 10. Realized prototype of the proposed FCPS.

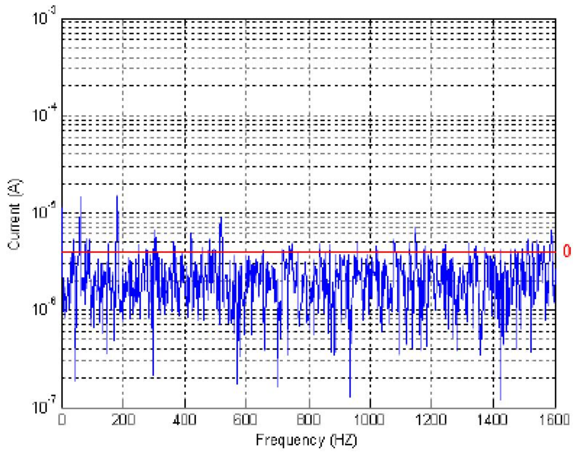

Figure 11. Measured output current spectrum of the proposed FCPS.

2017 JINST 12 T04004

5 Conclusions

The effectiveness of the FOFB greatly depends on the output performance of FCPSs. A rigorous mathematical modelling is very useful to shorten design time and improve design performance of a FCPS and therefore enhance the stability of beam orbit. By using the state-space averaging method, a rigorous mathematical modelling of the full-bridge FCPS in the FOFB of TPS was derived in this paper. The MATLAB/SIMULINK software was used to construct the proposed mathematical modelling and to conduct the simulations of the designed FCPS. The influence of different resolutions of ADC on the output accuracy of the FCPS was investigated. Simulation results showed that the proposed mathematical modelling is helpful for selecting the appropriate components to meet the accuracy requirements of the FCPS. Other optimal design issues such as the selection of circuit components, the adjustment of controller parameters, the influence of uncertainties in the current/voltage sensors and circuit components on the stability of FCPS and so on will be investigated in the future research.

References

[1] G.-H. Luo, *Overview of Accelerators Development at NSRRC*, Hsinchu, 18–22 January 2016 [online], http://www.icg.nsrrc.org.tw/felschool2016/lecture/2_Overview-of-accelerators-in-NSRRC.pdf.

[2] P.C. Chiu, K.H. Hu, C.H. Huang, C.Y. Liao and K.T. Hsu, *Preliminary Beam Test for TPS Fast Orbit Feedback System*, in *Proceedings of IPAC 2016*, Busan, Korea, pg. 2930–2932.

[3] K.L. Lian and P.W. Lehn, *Real-Time Simulation of Voltage Source Converters Based on Time Average Method*, *IEEE Trans. Power Syst.* **20** (2005) 110.

[4] B. Song and J. Wang, *Mathematical Modeling and Analysis of a Wide Bandwidth Bipolar Power Supply for the Fast Correctors in the APS Upgrade Controller*, in *Proceedings of IPAC 2015*, Richmond, VA, U.S.A. (2015), pg. 3264–3265.

[5] R.-S. Lai and K. Ngo, *A PWM Method for Reduction of Switching Loss in a Full-Bridge Inverter*, *IEEE Trans. Power Electron.* **10** (1995) 326.